Experimental Evaluation of Cover Plate and Flange Plate Steel Moment-Resisting Connections Considering Unequal Beam Depths

B.H. Hashemi[1*] and R. Ahmady Jazany[2]

1. Associate Professor, International Institute of Earthquake Engineering and Seismology (IIEES), Tehran, Iran, * Corresponding Author; email: behrokh@iiees.ac.ir
2. PhD Candidate, International Institute of Earthquake Engineering and Seismology (IIEES), Tehran, Iran

ABSTRACT

This paper presents the differences of cyclic behavior in Special Moment Resisting Frames (SMRF) with unequal beam depths which can be affected by connection detailing arrangements. The studied connection detailing arrangements consist of continuity plate arrangements such as straight or inclined continuity plates, coverplate and flange plate connection and haunch connection systems at the shallow beam side which can create some alternatives to connect shallow beams and deep beams with columns. In spite of probable occurrences of this special case in current engineering practice, codes do not take these especial cases into consideration. Six full scale beams to column sub-assemblages were tested to investigate the cyclic behavior for this special case i.e. unequal beam depths. Experiments show that the mentioned connection detailing arrangements could achieve performance discriminations ranged between story drift ratios of at least 4% to 6% radians before experiencing 20% strength degradation. Using a specific combination of flange plate connection with the haunch connection system, the crack propagation at the deep beam bottom flange which is observed in most of the connection detailing arrangements for this special case is eliminated.

Keywords:
Connection detailing;
Unequal beam depth;
Panel zone;
SMRF

1. Introduction

Since the 1994 Northridge earthquake, many moment connections have been proposed to develop ductile responses under cyclic loading. These post-Northridge beam-to-column connections, such as the introduction of a flange plate outside the beam flange [1-4] or a reduced section in the beam flange [4], are intended to force inelastic deformation of a beam away from the column face. Previous research has shown successful cyclic behavior of these connections and has been integrated into *FEMA* 350 [1]. Although post-Northridge connections recommended by *FEMA* 350 [1] achieve satisfactory performance, the field weld quality needed to assure adequate deformation of connections is difficult to control in practice. Since the Northridge earthquake, a great deal of research and testing has been conducted to identify better moment connections for new steel moment frame construction and for the repair or upgrading of existing steel moment frames. The majority of these efforts have combined improvements in welding together with modifications to the connection design. In many cases, the modified connection design calls for some types of reinforcement in the connection. Previous investigations were categorized on the effect of connection type, connection geometry, *PZ* behavior and material properties on the cyclic behavior of *SMRF* stated herein.

Experimental studies on *PZ* behaviour were initiated in the late 1960*s* and early 1970*s*, including research conducted by Krawinkler et al [5], Bertero et al [6], and later by Popov [7]. Results of a study by Tsai and Popov [8] indicated that panel zones designed according to *ICBO* [9] could undergo large inelastic shear distortion before reaching their rated shear capacity [10-11]. Weak *PZ* behaviour

may have played a role in the failures which occurred during the Northridge earthquake [12]. Lee et al [13] present the analytical model of dual *PZ* behaviour in haunch repaired steel for *SMRF*, and the results correlated well with *FEM* (finite element analysis) regarding initial secant stiffness, ultimate capacity and average dual *PZ* shear strain. In *FEMA*-355*D* [3], which originated from the *SAC* joint venture, the proposed method of design was substantially altered so that it became completely different to that specified in previous codes [14] based on the idea that the framing beams and panel zone should yield at the same time in order to achieve balanced behaviour. It defined the yield point of the beam and of the *PZ* as the base-line for this balanced condition. However, Jin and El-Tawil [15] were of the opinion that this method was unsatisfactory since such a balanced beam and *PZ* capacity could not guarantee controlled distortion of these elements, and that it would not be possible to establish simultaneous yield mechanisms in the beam and *PZ*.

The need for repairing the damaged moment resisting frame connections resulted in the use of a haunch connection system. Civjan et al [16] conducted an experimental program to evaluate methods of retrofitting existing steel moment connections for improved cyclic performance. Retrofitted specimens by haunch connection system were tested both with and without a composite floor slab for an interior column with equal beam depths. The tests showed poor performance of the bottom flange dogbone retrofit when the existing low toughness welds were left in place. Qi-Song et al [17] suggested a design method for the haunch connection system in order to minimize the stress concentration at the haunch tip. Chi et al [18] conducted full-scale cyclic testing of two pre-Northridge moment connections with simulated welding defects, and four rehabilitated moment connections for interior columns with equal beam depths were then tested to validate the proposed scheme. Both the experimental and analytical results showed that the use of the welded haunch and rib plates significantly reduced strain demands at the beam flange groove welds. Test results also showed that the inclination angle of the haunch, which was recommended to be within 30±5 degrees in an *AISC* Design Guide, can be extended to 50 degrees. Uang et al [19] investigated the cyclic performance of haunch repaired steel moment connections experimentally and numerically for exterior columns. Static and dynamic test results showed that the cyclic performance could be significantly improved when some modifications were made to the existing groove welded joint of the top flange and the plastic hinging of the beam occurred away from the face of the column.

Plate-reinforced connection was also another alternative to prevent high triaxial stress conditions close to the connection, for *SMRF*. Kim et al [20-21] experimentally studied the cyclic behaviour of five coverplate and five flange plate reinforced connections for exterior columns. The results indicated that the nonlinear behaviour of these types of connections is better than that of the unreinforced connections. There was also no brittle failure in these experiments, and all the test specimens had maximum beam plastic rotations of between 2.3% and 3.9% radians. Chung-Che Chou and Chia-Ching [22] studied the performance of steel reduced flange plate (*RFP*) moment connections for exterior columns, and evaluated the nonlinear behaviour of the *RFP* by means of nonlinear regression analysis. The results showed that there is outstanding performance for this type of connection, i.e. reduced flange plate (*RFP*) moment connections, compared to the flange plate connection (*FP*). Engelhardt and Sabol [23] performed twelve experiments with coverplate reinforced connections for exterior columns. Most of the investigated test specimens showed outstanding performance, and developed large plastic rotations. However, it should be noted that the provisions of FEMA-350 [1] emphasized that flange plates are superior to coverplates since the welding of a single plate, i.e. a flange plate connection, is more reliable than the welding of a combination of a beam flange and a coverplate.

Nakashima et al [24] performed 86 tests on full-scale beam-to-column connection sub-assemblies for exterior columns. The results of these tests showed that the ductility of the welded connections was affected by the type of run-off tab, but this result was not validated when the sub-assemblies were subjected to dynamic loading. El-Tawil et al [25] investigated the effect of the yield-to-ultimate stress ratio on the inelastic behaviour of pre-Northridge connections. The results of these experiments indicated the detrimental effects of high yield-to-ultimate stress ratios on the inelastic behaviour of such

connections. An experimental study by Dubina and Stratan [26] indicated that double bevel groove welds show better performance and superior cyclic behaviour to that of single bevel groove welds. Moreover, when the material strength was increased, the ductility of this type of connection decreased. Hopperstad et al [27] and Morquio and Reira [28] have indicated that there is no significant effect of strain rate on steel elongation. Dexter and Melenderz [29] performed an experimental study on forty small T-joint samples. The results of this study showed that high heat input welds and some detailing connections of the T-joint resulted in the triggering of the fracture, in spite of the high strain rate. The results also indicated that the lack of yielding in the through-thickness direction can be explained by the existence of triaxial constraint in the column flange material. Ricles et al [30] performed various experiments with the aim of improving the pre-Northridge detailing. This experimental work consisted of eleven full-scale specimens for exterior columns and thirty nine small-scale assemblies. The test results suggested that the use of weld metal with a minimum notch toughness of $27J$ at $-29^{o}C$ in conjunction with improved weld detailing including the removal of weld back bars could prevent weld line fracture and reduce fracture potential in welded moment frame connections. Anderson et al [31] showed that the application of weld overlays to the small size specimens resulted in a significant improvement in their cyclic performance. The plastic rotation capacity of both specimens was either close to or exceeded 3%. The application of weld overlays to the moment connection of the intermediate size specimen also improved the rotation capacity. Variations in the material properties lead to inaccurate prediction of weakness zones, and the use of weld filler metal with low notch toughness may result in premature failures of welds and improper geometry of the connection could intensify the high triaxial stress conditions and limit the uni-axial yield potential close to the connection [32-34]. Many of these brittle fractures were propagated into the column base metal, including fractures that appeared to scoop out some of the column material, referred to as mouse-ears or divots [35-36]. From the fractography that has been performed on these fractures [37-38], the primary cause of the fractures was identified as low-toughness weld filler metal combined with the existence of backing-bar notches and lack of fusion defects at the weld root. Many provisions [1-3] and codes [39] have presented the necessary requirements and sufficient detailing for the design and implementation of all types of connections, especially for *SMRF*. But there has not been any instruction or suggestion for the case of unequal beam depth for interior columns. Taking these conditions into account seems necessary when two spans with considerable different span lengths are adjacent and may result in the assignment of beams with different depths. On the other hand, there are also many alternatives to connect the deep beam and shallow beam together. Therefore, it creates a complexity for the designer to choose a proper detailing, especially for *SMRF* in seismic areas. With due regard to many consultant companies schemes and experiences from the point of view of the authors and other professional engineers views, it is observed that designers use beams with equal depths when encountered such a condition and avoid presenting a scheme and specific detailing for this special case. In spite of the differences between the two cases, i.e. joint with unequal beam depths and equal beam depths, this study tries to investigate the cyclic response regarding differences in connection detailing for this special case and compare different detailing analytically experimentally.

2. Description of the Experimental Studies

2.1. Test Set Up Description and Loading Test Protocol

In order to develop the understanding of *SMRF* cyclic behavior with unequal beam depth, six experiments were conducted in full scale for interior column and unequal beam depth. To simulate the actual conditions of *SMRF*, six sub-assemblages with different connection detailing arrangements were considered. The sub-assemblages were full-scale simulations of an *SMRF*. They were extracted from the frame assuming that the inflection point is at the mid-point of all the elements. The experimental program was performed to provide a comprehensive understanding of the cyclic behavior of the *SMRF* with unequal beam depths. Figure (1) shows the test setup, including reaction supports and out of plane buckling supports for the beams. The bottom ends of the column were pinned to the strong floor of the laboratory, and out-of-plane buckling prevention devices were installed at the mid-point of the beam spans.

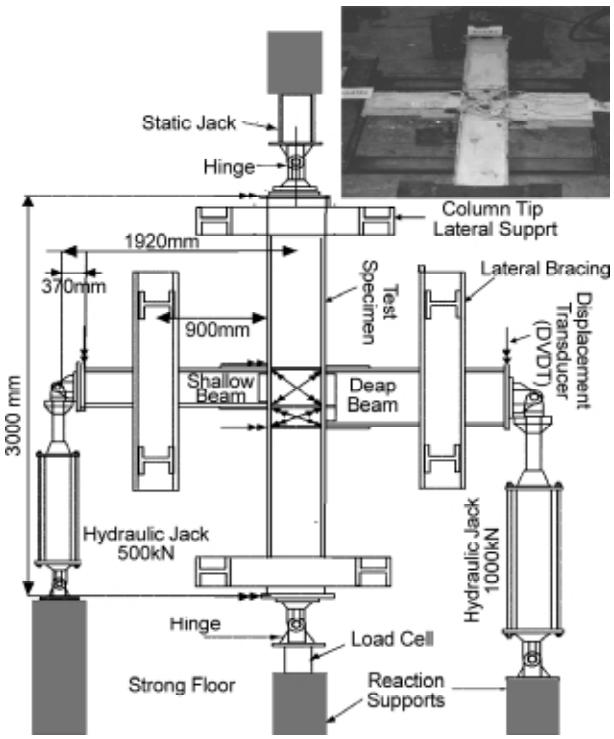

Figure 1. Schematic view of test set up.

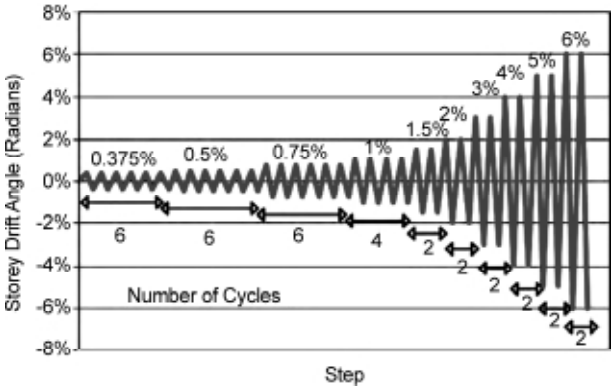

Figure 2. Schematic view of load pattern [39].

Two hydraulic actuators for simulation of the seismic load were applied on the specimens' beam tips which were fixed on the strong floor of the structural laboratories. One of the hydraulic actuators was capable of applying loads up to $1000kN$ and a stroke of up to $\pm 150mm$ for the deep beam, and another was capable of applying loads up to $500kN$ and a stroke of up to $\pm 150mm$ for the shallow beam. The story drift angle of 0.01 radians corresponded to the displacement of $20mm$ at a hinge of hydraulic jack. Figure (2) shows the displacement load pattern which originated by the *AISC* seismic provisions load pattern [39]. This load pattern was applied for the beams' tip in a reverse direction and in a plane situation to simulate seismic excitation. A constant axial load equal to 40 tons was applied and measured by a static jack and load cell to the top and bottom of the column ends respectively (this value corresponds to a compressive stress value of $0.3fa$, where fa is the column's allowable compressive stress) in order to simulate the axial load effects.

2.2. Instrumentation

Test specimens were equipped with a combination of displacement transducers, triaxial strain gauges (rosettes) and uniaxial strain gauges to measure the elastic and inelastic deformations and strain locally. The displacement transducers were applied for the column tips and beam to column intersections to measure column rotation. Some transducers are also used diagonally to measure *PZ* shear strain. In order to monitor the inelastic deformation visually during the test, whitewash was painted on the specimens. Figure (3) shows the connection detailing arrangements for every specimen and also indicates the weld detail. Seven strain gauges were installed on every specimen and are called No. 1-7. Strain gauges No. 1-6 were uniaxial, their direction of measurement being parallel to the main axis of the beams, whereas the strain gauge No. 7 was a triaxial rosette, see Figure (3), which its main directions of measurement being parallel to the main axes of the beams and, orthogonally, parallel to the main axis of the column. The strain gauges are marked by bold lines (-) except for strain gauge No. 7, marked by an asterisk (*), and by their serial numbers (1-7), see Figure (3). The column length was $300cm$ and the length of each beam (the distance from the main column axis to beam tips) was $155cm$. The distance between the hinged joints, located on the axes of the lateral hydraulic jacks, and the ends of the shallow and deep beam was $37cm$, as shown in Figure (1). This value was considered in all the calculations.

2.3. Material Properties, Construction Process and Design Criteria for the Test Specimens

The coupon tensile test of steel material was conducted. The material properties, continuity plate arrangements and connection type are summarized in Table (1). In order to join the elements, i.e. beam and column, the *CJP* groove weld with different

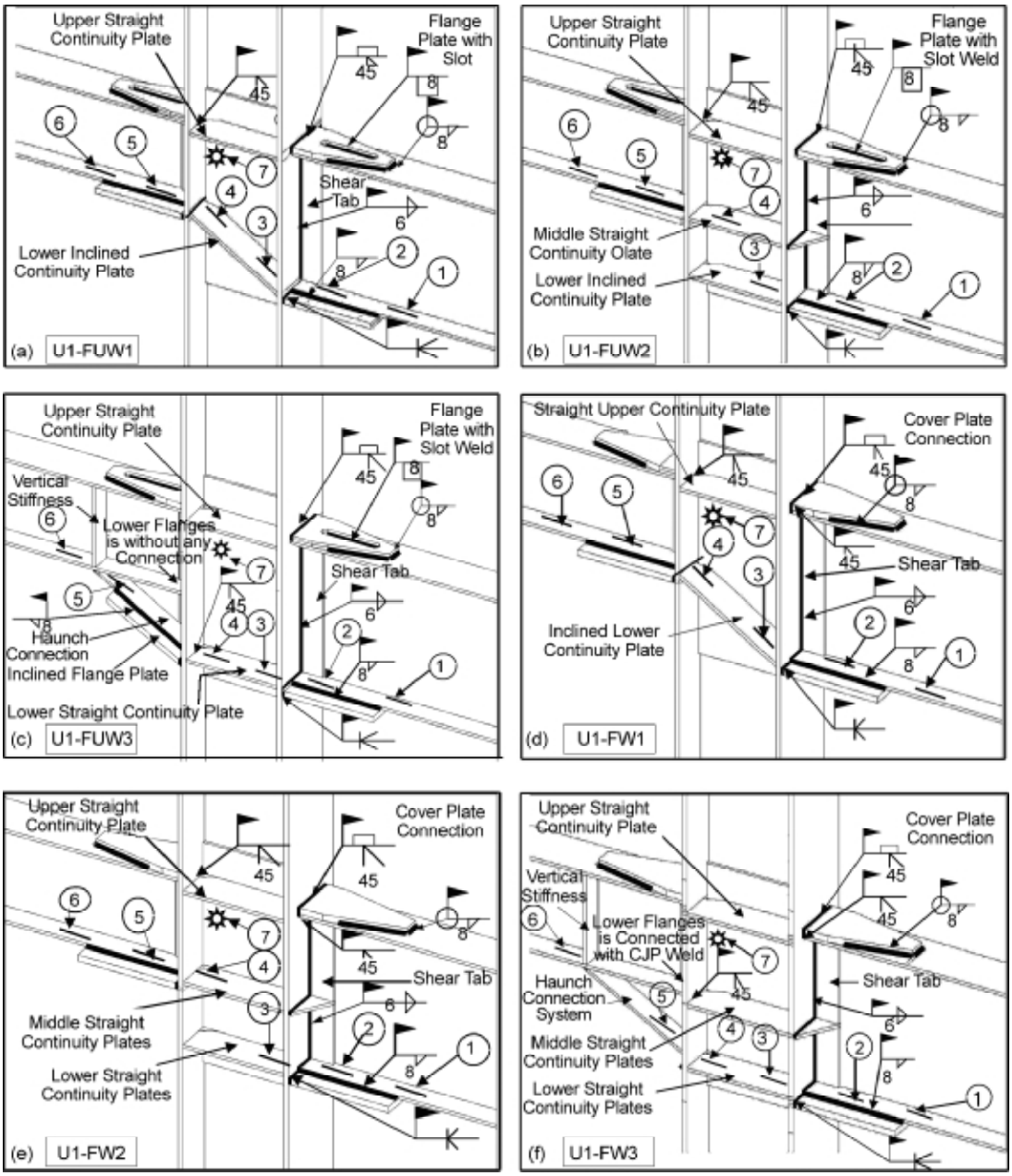

Figure 3. Connection detailing arrangements for six specimens (the serial numbers (1-7) with bold line (-) and asterisk (*) are uniaxial and triaxial strain gauge locations respectively).

Table 1. Data about the investigated test specimens.

Specimen Name	Beam	Column Flanges	Column Web	Doubler Plates	Weld (6013,4*mm*)	Lower Continuity Plate Arrangement and Number of Lower Continuity Plates	Connection Type
	F_y F_u	F_y F_u	F_y F_u	F_y F_u	F_y F_u		
*U*1-*FUW*1	230.3 373.8	269.2 390.1	245 373.8	260.5 385	460 522	Inclined (1)	Flange Plate
*U*1-*FUW*2						Straight (2)	Flange Plate
*U*1-*FUW*3						Straight (1)	Flange Plate
*U*1-*FW*1						Inclined (1)	Coverplate
*U*1-*FW*2						Straight (2)	Coverplate
*U*1-*FW*3						Straight (2)	Coverplate
Units: MPa							

methods of construction regarding welding positions was used. Figure (4) shows general connection detailing and element section dimensions, i.e. beams and column, used for the specimens such as coverplate and flange plate dimensions, haunch detailing and continuity plate connection. The deep beam flange is hereinafter referred to as "Beam 50" and the shallow beam, is referred to as "Beam 30".

To construct the elements of the specimens such as beam and column, the built-up *I* shaped with continuous fillet weld line at both sides of plate with *E*6013 welding electrode was used. The welding process was Shielded Metal Arc Welding (*SMAW*) both for fillet weld and *CJP* weld. For the

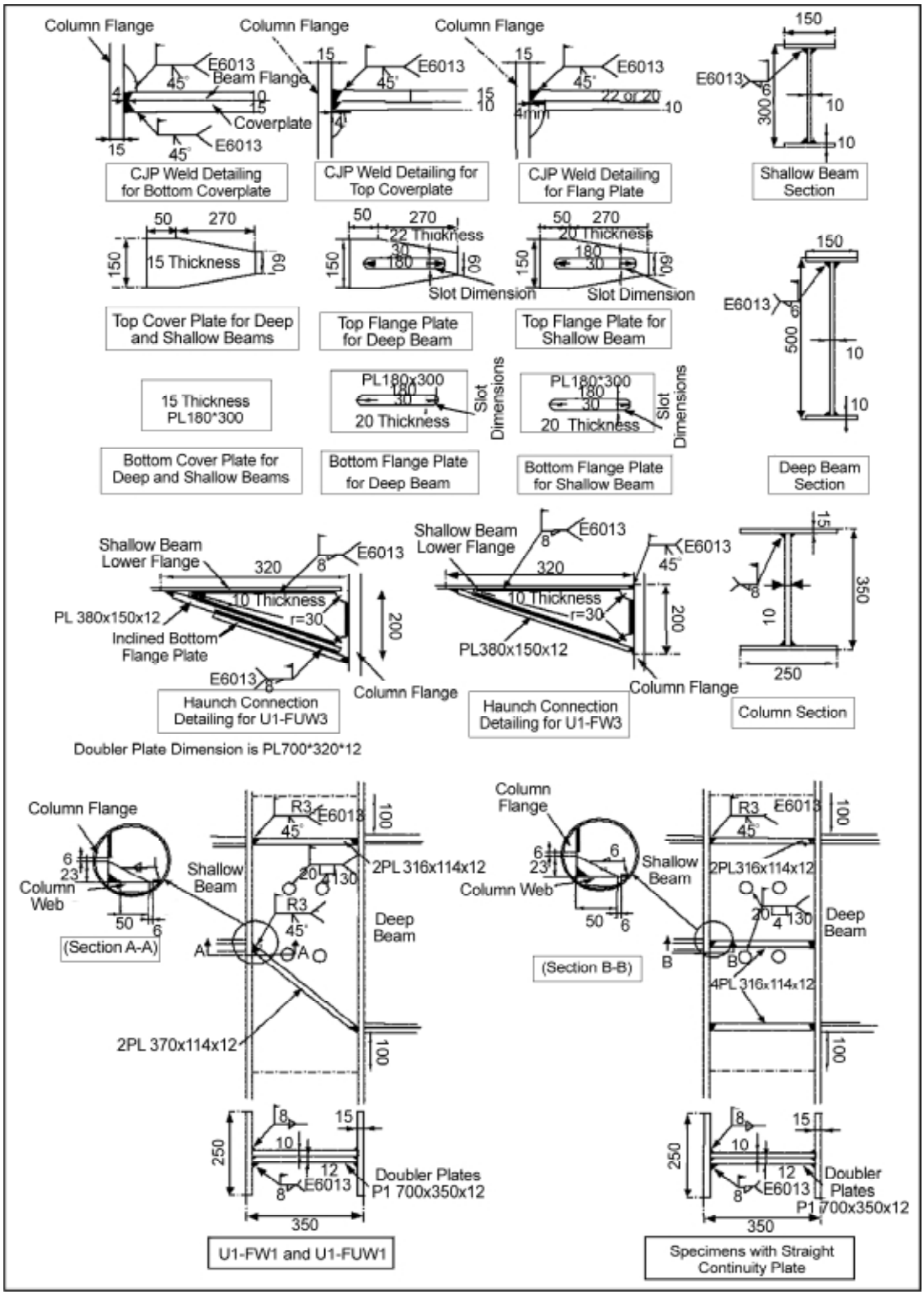

Figure 4. Section details of the test specimens (The dimensions are in millimeter).

QC (quality control) of the welding process, the visual inspection and *PT* (penetration test) were conducted. In order to facilitate full penetration of weld filler metal, *E*6010 welding electrode was used for root pass and then *E*6013 welding electrode with a diameter of 4*mm* was used. The charpy *V* notch test for welding electrode was also performed based on our order from the manufacturing company (*AMA*^{TM} *Co.*). Based on the data of the mentioned test, the welding electrode had minimum charpy *V* notch 29 at minus 29°*C*, which satisfies the minimum requirement of code (*AWS*) for the *CJP* weld process [2, 39, 40].

The doubler plates and connection design were set according to *AISC* seismic provisions [39]. Moreover, it was designed to meet the balance conditions of beam and *PZ* according to *FEMA* 355-D [3]. Table (2) presents a summary of design regarding *AISC* [39]. Based on these provisions, the dimensions of the doubler plates were 70x32x1.2*cm*. The connection detailing, including flange plate and coverplate were designed according to *AISC* [39] [41], and some suggestions from *FEMA* 355-*D* [3] and *FEMA* 350 [1] were also considered for the mentioned connections (coverplate and flange plate).

In the experimental work of the present study, some limitations have been imposed by laboratory; some of which consists of: (1) similar and constant lengths between inflection points and the column face while it could be non-similar and non-constant in actual conditions (2) the absence of the concrete slab (3) the constant value of the axial load which is not constant with regard to different spans lengths for beams with unequal beam depths and number of stories. These limitations could affect the cyclic responses of beams, *PZ* and actual behaviour of test specimens; however, the focus of this study is considering the effect of detailing on *SMRF* cyclic behaviour and the results can just show the comparative aspects of detailing effects in order to improve seismic performance of the *SMRF* for these special cases, .i.e. unequal beam depth.

Table 2. Design summary [39].

Design Criteria(The Parameters are Referred to AISC [39])				
Weak Beam-Strong Column Ratio (ASD)	$\frac{\sum M_{pc}}{\sum M_{pb}} \geq 1 \rightarrow 1.11$	$M_{pb} = \sum (1.1/1.5 R_y F_{yb} Z_b + M_{ov}) = 377kN$ $M_{pc} = \sum Z_c (.66F_{yc} - P_{uc}/A_g) = 420kN$		
PZ Requirement (AISC 2005-ASD)	$V_{cp} = (0.6/1.5) F_y d_c t_{cw} (1 + \frac{3b_{cf} t_{cf}^2}{d_b d_c t})$ $V_{pd} = \frac{M_1}{d_{b1}} + \frac{M_2}{d_{b2}} - V_{col} \rightarrow$	$V_{cp} - 790(kN) \geq V_{pd} - 710(kN)$ $t_{dp} = 12mm$		
Continuity Plate Requirement (ASD)	$A_{st} = \frac{P_{bf} - F_{yc} t_{wc} (t_b + 5k)}{F_{yst}}$ $\rightarrow A_{st} = 16.5cm^2$	$t_{cf} \leq 0.54 \sqrt{b_{fb} t_{fb} F_{yb} / F_{yc}} \rightarrow$ $t_{cf} \leq b_f / 6 \rightarrow$	$1.5 \geq 1.46$ $1.5 \leq 2.5$	(Regarding AISC 2005) Continuity Plate Thickness: $t_{cf} = 10mm$: Straight Continuity Plate $t_{cf} = 12mm$: Inclined Continuity Plate
Flange Plate Requirement (ASD)	$V_u = 2(1.1 R_y M_p)/l_h, M_c = 1.1 R_y F_y bt$ (b, t are Section Dimensions of Flange Plate) (Refer to AISC [39] (Section 9))		$t_{fp} = 22mm$: for Deep Beam $t_{fp} = 20mm$: for Shallow Beam	
Cover Plate Requirement (ASD)	Based on FEMA-355D [3] and AISC [39]: $t_{cp} = 15mm$			

Beam and Column Properties	$Z_x (cm^2)$	$S_x (cm^2)$	Demand at the Face of Column (kN.m) (LRFD)	Demand at the Face of Column (kN.m) (ASD)
Deep Beam Properties	1313	1089	398	236
Shallow Beam Properties	601	542	180	97
Column Properties	1584.75	1359.25	Applied Axial Load Stress = 0.3 f_a (f_a is Column's Allowable Compressive Stress)	

3. Test Specimens Descriptions

Test specimen *U*1-*FUW*1 consisted of a trapezoidal top flange plate connection and a rectangular bottom flange plate at the shallow beam (beam 30) and deep beam (beam 50) with an inclined lower continuity plate, which was fitted to meet the beams' bottom flanges as shown in Figure (3a). To provide enough weld line in accordance with *FEMA*-350 [1], a slot weld was used for both the top and bottom flange plates. For the bottom flange plate, the slot welding was performed in overhead positions in the experiment similar to actual constructional conditions. Test specimen *U*1-*FW*1 was similar to *U*1-*FUW*1, but a coverplate connection was used for this test specimen instead of a flange plate, as shown in Figure (3d). Test specimens *U*1-*FUW*2 and *U*1-*FW*2 were similar to *U*1-*FUW*1 and *U*1-*FW*1, respectively, except for the lower straight continuity plate and middle continuity plates, which were used for these test specimens instead of inclined continuity plates, as shown in Figures (3b) and (3e), respectively.

The test specimen *U*1-*FUW*3 consisted of a flange plate connection with a slot weld on the deep beam side, including the top and bottom flange plate connection. The assemblage of the shallow beam and haunch system is connected to the column flange by a top flange plate and an inclined bottom flange plate, which is connected to the haunch flange by a fillet weld line as shown in Figures (3c) and Figure (4). The advantages of using an inclined flange plate are: (1) it is possible to assemble the shallow beam and haunch system away from the column erection site and (2) the welding of shallow beam bottom flange to haunch web connection can be performed in the horizontal or flat position. Because the shallow beam bottom flange is not directly connected to the column flange, a middle straight continuity plate was not necessary, see Figure (4). This detailing is the innovative scheme of the ensemble, which is not used in practical engineering and has not been mentioned in other provisions and codes such as *FEMA* 350[1], *FEMA* 355-*D* [3] and *AISC* 2005 [39, 41].

As shown in Figure (3f), test specimen *U*1-*FW*3 consisted of a coverplate connection on the deep beam side, including a top and bottom coverplate connection, whereas for the shallow beam, a top coverplate connection was used and a bottom coverplate was not used for the bottom flange. The shallow beam bottom flange and haunch flange were directly connected to the column flange by a *CJP* groove weld, as shown in Figure (4). A middle straight continuity plate was necessary in this test specimen at the location of the beam's bottom flange because of the *CJP* groove weld connection at shallow beam's bottom flange.

4. Experimental Results

4.1. Methods of Beam Response Normalization and PZ Shear Measurement

In this study, the global behavior of the experiment consisted of the normalized deep beam moment $(M_D / C_{pr}.Z_D.F_{ye})$ and normalized shallow beam moment $(M_S / C_{pr}.Z_S.F_{ye})$ at the face of the column versus story drift angle for all specimens. Where Z_D and Z_S are the plastic section modulus of deep beam and shallow beam, respectively. F_{ye} is the measured expected yield stress of the beams' material, M_D and M_S are applied moments at the column face for the deep beam and shallow beam respectively, and C_{pr} is a factor to account for the peak connection strength, including strain hardening, local restraint and additional reinforcement [1].

Also, θ is story drift angle [42] computed by dividing the beam tip displacement by the distance from the actuator hinge axis to the column centerline. The total normalized moment $((M_D + M_S)/(C_{pr}.Z_S.F_{ye} + C_{pr}.Z_D.F_{ye}))$ [42] versus shear strain of $PZ(\theta_{pz})$ for every specimen is also presented in this section. The method of *PZ* shear strain (θ_{pz}) calculation varies for the different test specimens. In the case of specimen *U*1-*FUW*3, the shear strain of $PZ(\theta_{pz})$ can be calculated from the following equation [42]:

$$\theta_{pz} = \frac{\sqrt{a^2 + b^2}}{2ab}(\Delta_1 - \Delta_2) \quad (1)$$

where *a* and *b* are the horizontal and vertical boundary lengths of *PZ* respectively, Δ_1 and Δ_2 are measured data of displacement transducers installed diagonally as shown in Figure (5). In the case of test specimens *U*1-*FW*2, *U*1-*FUW*2 and *U*1-*FW*3, there are, in fact, two separate panel zones. The weighted average value of the shear strain of the panel zone upper and lower segments can be calculated from the following equations [42]:

$$\theta_{pz} = \frac{b.\theta_{lower-pz} + c.\theta_{upper-pz}}{b + c} \quad (2)$$

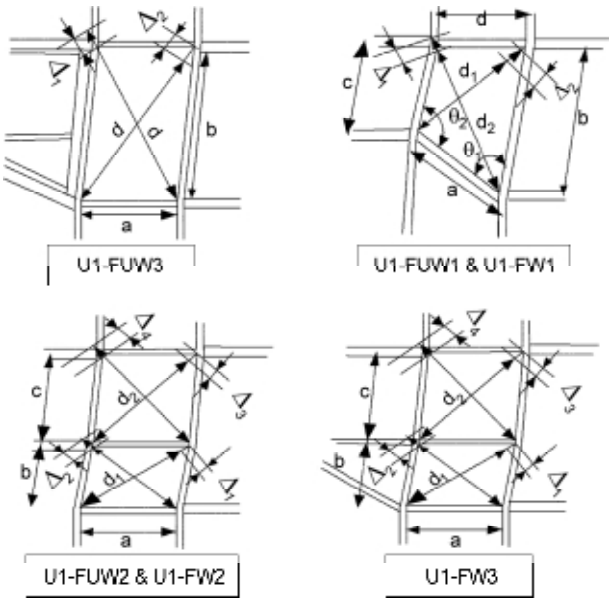

Figure 5. Measurement detailing of the PZ for the test specimens.

$$\theta_{lower-pz} = \frac{\sqrt{a^2 + b^2}}{2ab}(\Delta_1 - \Delta_2) \quad (3)$$

and

$$\theta_{upper-pz} = \frac{\sqrt{a^2 + c^2}}{2ac}(\Delta_3 - \Delta_4) \quad (4)$$

where $\theta_{lower-pz}$ and $\theta_{upper-pz}$ are the shear strains of the panel zone lower and upper segments respectively; *a*, *b*, and *c* are the corresponding lengths of the boundaries of the panel zone upper and lower segments, see Figure (5); and $\Delta_1, \Delta_2, \Delta_3$, and Δ_4 are the data obtained by measurements using *LVDT's*, installed diagonally across the panel zone. In the case of test specimens *U*1-*FW*1 and *U*1-*FUW*1, due to the presence of an inclined continuity plate along the lower boundary of the *PZ*, the latter's shape is trapezoidal. The method calculation of the *PZ* shear strain is different from the other two test specimens. Based on the geometrical rules, the *PZ* shear strain can be computed as follows:

$$\theta_{pz} = \frac{1}{4}\left(Arc\sin\frac{\Delta_1(2d_1+\Delta_1)}{ab.\sin(\theta_1)} - Arc\sin\frac{\Delta_2(2d_2-\Delta_2)}{ac.\sin(\theta_2)}\right) \quad (5)$$

where, see Figure (5), a, b and *c* are the *PZ* boundary lengths, θ_1 and θ_2 are the angles which the inclined continuity plate makes with the column flanges, d_1 and d_2 are the main diagonals of the trapezoidal *PZ*, Δ_1 and Δ_2 are the data obtained by measurements using *LVDT's*, installed diagonally across the panel zone.

4.2. Test Observations

4.2.1. Test Specimen U1-FUW1

Test specimen *U*1-*FUW*1 underwent elastic response in the first 20 cycles (the 20^{th} cycle corresponded to story drift angle of 1.0%) of loading. Based on the strain gauge data fixed to the *PZ*, the *PZ* yielding started at the corners which was close to the shallow beam at the 21^{st} cycle (at 1% drift), then the deep beam yielded away from the column flange nearly at the 22^{nd} cycle (at 1.5% drift). Local deep beam bottom flange buckling occurred at a 4% and 5% story drift ratio and yet no local buckling of the web was observed at the deep and shallow beam plastic hinge region. Test specimen *U*1-*FUW*1 underwent severe inelastic behavior at cycle 34, which corresponds to the story drift angle of 0.06 radians and the local bucking at deep beam web close to the bottom flange and deep beam bottom flange occurred, see Figure (6). Thus, in order to prevent apparatus damage, the test was terminated. During the test, no flange and web buckling was observed at the shallow beam side. The hysteresis behavior of *U*1-*FUW*1 for deep beam and *PZ* are presented in Figures (7) and (8), respectively. The degradation of strength and stiffness is evident in Figure (7) that is due to flange and web local buckling at the plastic hinge zone of the deep beam web and deep beam bottom flange. The degradation value computed at story drift angle of

Figure 6. (a) Specimen U1-FUW1 erected after the experiment (rear view) (b) Deep beam flange buckling (front view) (c) view of fixed equipment for specimen U1-FUW1 during the test (front view).

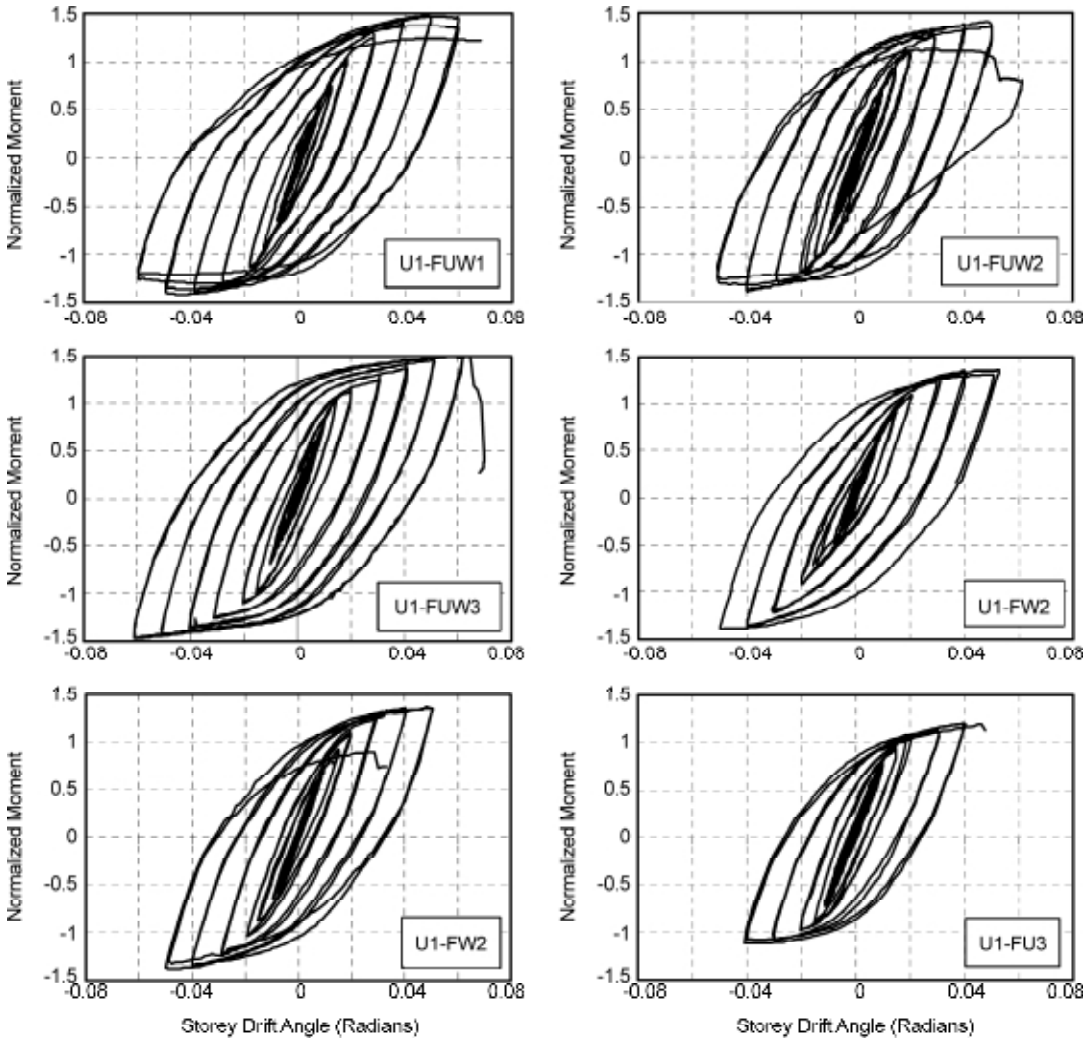

Figure 7. Plots of deep beam's cyclic response of the test specimens.

0.04 radians at the deep beam in the case of specimen *U*1-*FUW*1 reaches 16%, which satisfies the strength degradation limit criteria with regard to *AISC* [39].

The deep beam and shallow beam section for all specimens were compact in flange and web in accordance with *AISC* seismic provisions [41], thereby the delayed degradation was expected. Based on the measured strain and seismic response of shallow beam, in the case of test specimen *U*1-*FUW*1, the shallow beam did not enter nonlinear behavior significantly. Figure (6) shows this specimen at the end of the test.

4.2.2. Test specimen U1-FUW2

During the first 21 cycles (the 21^{st} cycle corresponded to story drift angle of 1.0 %), the behavior of test specimen *U*1-*FUW*2 was also in the elastic range. The *PZ* yielding started at the 23^{rd} cycle at the corners which were close to the deep beam (at 1.5% drift), but deep beam yielding started earlier, and the deep beam bottom flange of test specimen *U*1-*FUW*2 experienced local buckling at story drift angle of 0.04 radians. This phenomenon was coincident with deep beam web buckling and shallow beam bottom flange buckling at a story drift angle of 0.05 radians. Fracture of deep beam flange close to the end of the flange plate occurred at a story drift angle of 0.05 radians and the test was terminated, see Figure (9). Regarding the strain gauge data and whitewashed area, the plastic hinge mechanism is also evident at the upper *PZ* segment, deep beam and shallow beam side. Figure (7) shows strength degradation of the deep beam response of specimen *U*1-*FUW*2, which is an indicator of deep beam flange buckling, and the degradation reaches a value of 12 %. Figure (8) also shows the *PZ* response of this specimen.

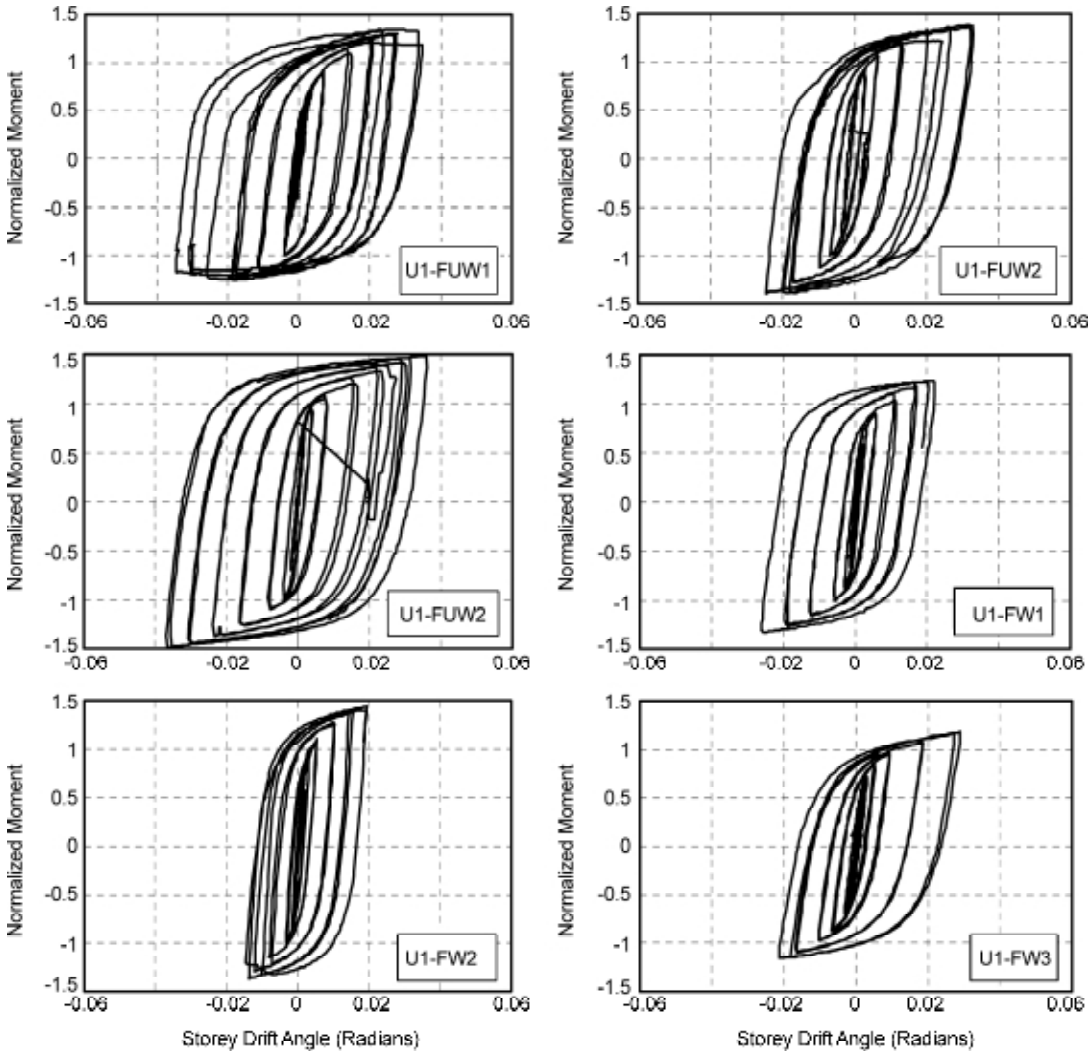

Figure 8. Plot of PZ's cyclic response of the test specimens.

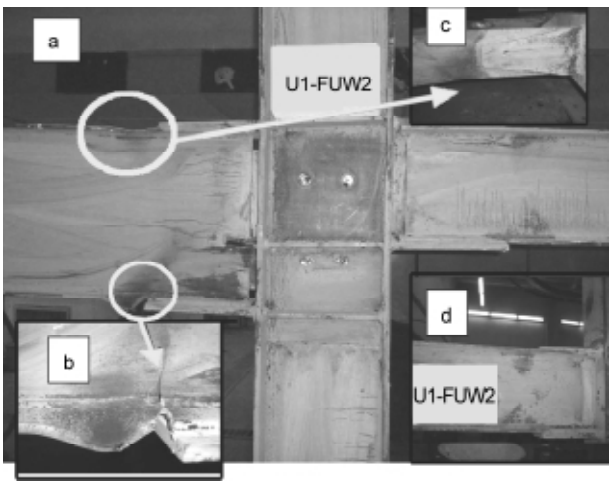

Figure 9. (a) View of specimen U1-FUW2 erected after the experiment and flaking of whitewashed area at deep and shallow beam and PZ upper segment (rear view) (b) deep beam bottom flange fracture (rear view) (c) deep beam top yielding area (top view) (d) flaking of whitewashed area at the shallow beam (front view).

4.2.3. Test Specimen U1-FUW3

Test specimen *U*1-*FUW*3 also showed elastic behaviour during the first 22 cycles (the 22^{nd} cycle corresponded to story drift angle of 1.5%). Regarding strain gauge data, deep beam, shallow beam and *PZ* underwent nonlinear behavior at the 23^{rd} cycle (with 1.5% drift). The substantial inelastic deformation took place beyond the end of the flange plate connections as shown in Figure (10) at the 34^{th} cycle, which was equal to a story drift angle of 0.06 radians. During the test, no significant flange buckling and web local buckling was observed; hence, the degradation of strength and stiffness are not observed in the cyclic response of deep beam in this specimen as shown in Figure (7). Moreover, the large whitewashed area of the deep beam, shallow beam and the entire area of *PZ* flaked off. In order to prevent apparatus damage, the test was terminated

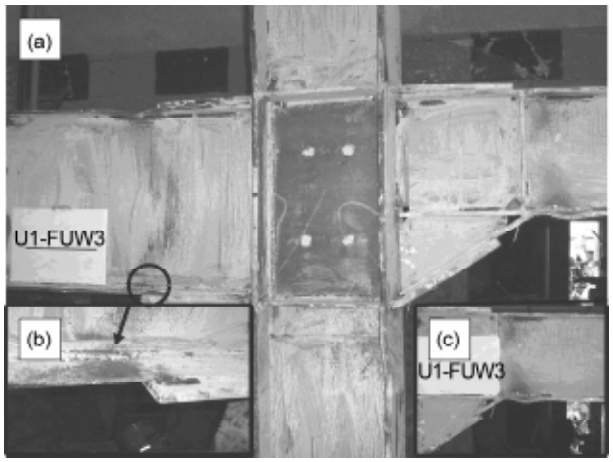

Figure 10. (a) Test specimen U1-FUW3 and flaking of whitewashed area after the test (rear view) (b) deep beam bottom flange without any rupture (rear view) (c) flaking of whitewashed area at shallow beam with haunch connection system.

at a story drift angle of 0.06 radians. The crack initiation or rupture was not observed in all elements of these specimens. The main idea of reinforcing the connection using flange plate or coverplate is in relocating the plastic hinge away from the face of the column into the beam beyond the reinforcing plate which was observed in the specimens of this study. Figure (10) illustrates a large plastic hinge region of deep beam, shallow beam and *PZ*.

4.2.4. Test Specimen U1-FW1

Test specimen *U*1-*FW*1 experienced elastic response within the first 21 cycles (the 21^{st} cycle corresponded to story drift angle of 1.0 %). Similar to specimen *U*1-*FUW*1, the *PZ* of this specimen yielded earlier than the beams. The specimen *U*1-*FW*1 underwent inelastic behavior, but there were not significant web and flange buckling at a story drift angle of 0.04 and 0.05 radians corresponding to the 30^{th} and 32^{nd} cycles. Deep beam bottom flange rupture suddenly occurred at a story drift angle of 0.05 radians, and the test was terminated. The measured strain gauge at the shallow beam and its response indicated that there was little inelastic behavior at the expected plastic hinge region beyond the end of the coverplate like specimen *U*1-*FUW*1. Based on measured strain values on the shallow beam and its response, in the case of test specimen *U*1-*FW*1, the shallow beam hardly entered a nonlinear range, whereas the deep beam went through a nonlinear range considerably.

4.2.5. Test Specimen U1-FW2

Specimen *U*1-*FW*2 indicated elastic behavior within the first 21 cycles (the 21^{st} cycle corresponded to story drift angle of 1.0 %) and the deep beam started to yield at the 22^{nd} cycle (at 1.5% drift), and the *PZ* upper segment yielded at the 23^{rd} cycle. The specimen underwent inelastic behavior without any significant buckling at beam flanges and web, and there is no degradation in the hysteresis behavior of the deep beam as shown in Figure (7). The specimen failed due to deep beam bottom flange fracture at a story drift angle of 0.05 radians, and the test was terminated.

4.2.6. Test Specimen U1-FW3

Test specimen *U*1-*FW*3 showed the worst response regarding the value of story drift angle than all other specimens, resulting in poor performance. This specimen experienced elastic behavior within the first 21 cycles (the 21^{st} cycle corresponded to story drift angle of 1.0%), and the deep beam started to yield at the 22^{nd} cycle (at 1.5% drift) and then *PZ* yielded one cycle later. The deep beam bottom flange buckling happened at a story drift angle of 0.03 radians. The specimen underwent inelastic behavior at a story drift angle of 0.04 radians, and the deep beam bottom flange fractured at a story drift angle of 0.04 radians as shown in Figure (11). According to the measured strain values at the beams flange, the shallow beam and deep beam, see Figure (7), entered a nonlinear range significantly, based on flaking of the whitewashed area at the shallow beam. The plastic hinge length of the shallow beam was short compared to specimen *U*1-*FUW*3.

4.3. Considering the Strain Gauge Data

Figure (12) shows maximum measured strain values versus the points as shown in Figure (3). Based on this Figure, the deep beam bottom flange of specimen *U*1-*FW*2 had maximum measured strain values (44000 microstrains). The specimen *U*1-*FUW*1 had a minimum value of measured strain, and the deep bottom flange reached a value of 31000 microstrains. The corresponding values for the deep beam of specimens *U*1-*FUW*2, *U*1-*FUW*3, *U*1-*FW*1, and *U*1-*FW*3 reach values of 42000, 33000, 35000 and 40000 microstrains, respectively. The shallow beam bottom flange measured strain

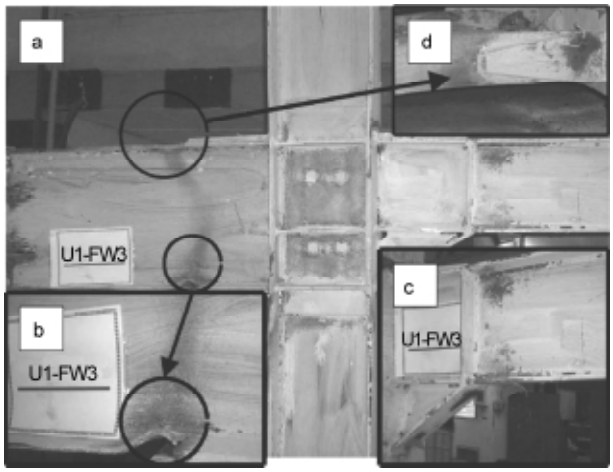

Figure 11. (a) Specimen U1-FW3 erected after the experiment (rear view) (b) deep beam bottom flange fracture (rear view) (c) flaking of whitewashed area at shallow beam (rear view) (d) flaking of whitewashed area at deep beam top flange beyond the coverplate (top view).

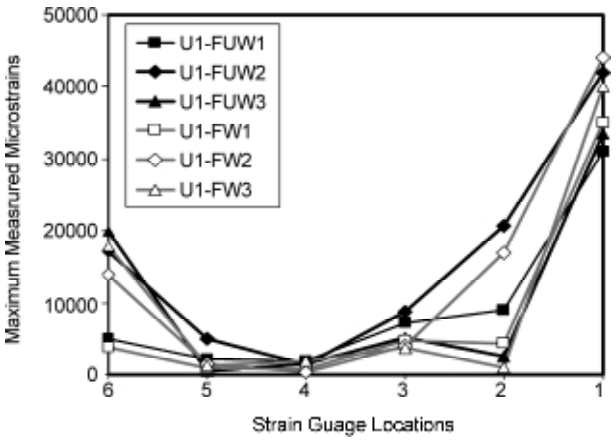

Figure 12. Maximum measured strain demand for uniaxial strain gauge locations and all the test specimens.

values of specimen *U*1-*FW*1 and *U*1-*FUW*1 with inclined continuity plate values of 3900 and 5000 microstrains, which are the least values among these specimens. The rest of the specimens had at least three times that of the corresponding values compared to specimen *U*1-*FW*1. This shows that inclined continuity plate arrangement leads to a slight entrance of shallow beam to the nonlinear range. On the contrary, the shallow beam of the specimens with the haunch connection system, i.e. specimens *U*1-*FUW*3 and *U*1-*FW*3, provide more acceptable and balance conditions compared to the other specimens in order to enter a nonlinear range significantly. Also, the shallow beam of specimens with straight continuity plate arrangement, i.e. specimens *U*1-*FUW*2 and *U*1-*FW*2, provide approximately similar conditions compared to test specimens with the haunch connection system. Figure (13) shows measured strain values versus story drift angle at the deep beam bottom flange plate (for test specimens *U*1-*FUW*1, *U*1-*FUW*2 and *U*1-*FUW*3) and coverplate (for test specimens *U*1-*FW*1, *U*1-*FW*2 and *U*1-*FW*3), i.e. location of No. 2, as shown in Figure (3).

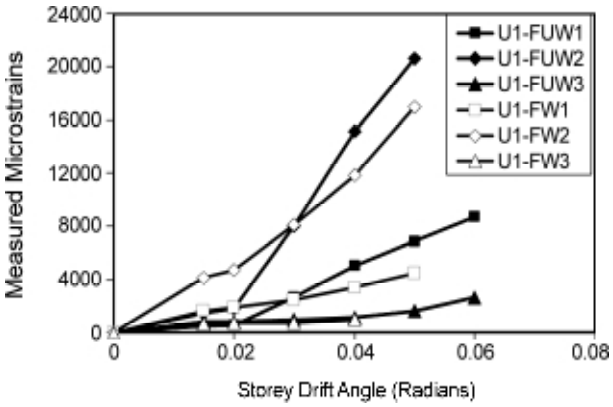

Figure 13. Measured strain demand at location No. 2 vs. story drift angle (the measured direction for this diagram is parallel to the main axes of the beams).

Based on the mentioned diagram, specimens with straight continuity arrangements, i.e. specimens *U*1-*FW*2 and *U*1-*FUW*2, have maximum measured strain values on the deep beam bottom flange plate and deep beam bottom coverplate, respectively at a story drift angle of 0.05 radians. Moreover, measured strain values of specimens with inclined continuity plates, i.e. *U*1-*FUW*1 and *U*1-*FW*1, at the deep beam bottom flange plate and coverplate are in the middle range compared to the rest of the specimens, also in the cases of test specimens with haunch connection system, i.e. specimens *U*1-*FUW*3 and *U*1-*FW*3, have the least strain values for the deep beam bottom flange plate and coverplate respectively. This diagram also shows that the connection detailing arrangement has a direct influence on stress concentration values, even at deep beam bottom coverplate and flange plate connections. This diagram also shows that test specimens with the haunch connection system for unequal beam depths, i.e. specimens *U*1-*FUW*3 and *U*1-*FW*3 could provide the least stress concentration values at deep beam connections than the others.

Figure (14) shows the local shear strain values versus the normalized total moment for all specimens which have been derived from the rosette strain gauge at location No. 7. Based on this Figure, specimen *U*1-*FW*2 which had the smallest values of global *PZ* shear strain than the others, as shown in Figure (3), shows the largest local shear strain values close to the doubler plates weld-line and reached a value of 30000 microstrains. This shear strain value could not be a proper strain state for the doubler plates weld-line, since severe local shear distortion in the proximity of the weld-line could increase the weld-line rupture probability. Specimen *U*1-*FW*3 had the least local shear strain values at the mentioned location (i.e. location No. 7) and reaches 5000 microstrains. The rest of the specimen indicates local shear strain discriminations at location No. 7, ranging between values of 10000 to 150000 microstrains.

5. Considering PZ Seismic Behavior for the Test Specimens

In this study, *PZ* detailing was designed according to *AISC* [39]. *PZ* requirements were also adjusted to provide the balance conditions according to *FEMA*-355*D* [3]. For a connection, the balance conditions are provided where the total transferred flexural yield capacity of the beams which are projected at panel zone centre (V_{PZMy}) should be equal to 0.9 of *PZ* shear yield capacity (V_y) i.e. $V_{PZMy}/V_y = 0.9$. These provisions suggest that $0.6 \le V_{PZMy}/V_y \le 0.9$ is a safe margin to prevent excessive stress concentrations in the connection or excessive deformation and potential fracture of the connections, also including the *PZ* energy dissipation potential. It should be noted that the doubler plates thickness used in the described experimental work corresponds to the upper threshold of this criterion, i.e. (the exact value for all test

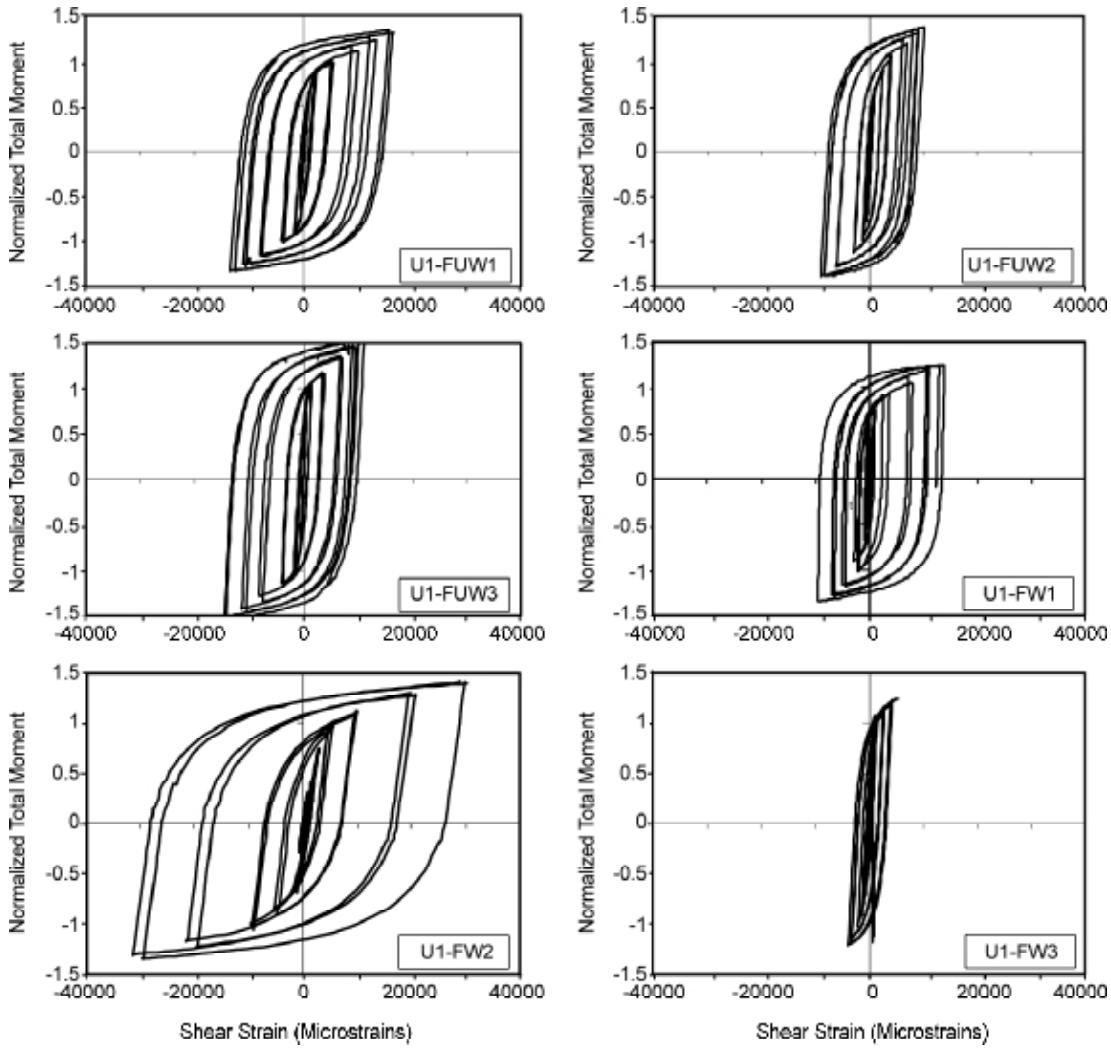

Figure 14. Normalized total moment versus local shear microstrains for different specimens at location No. 7.

specimens regarding test data in the experiment is 0.87). Based on the above-mentioned description, the beam flexural yielding should be coincident with *PZ* shear yielding and the observations approximately confirmed this issue.

The *PZ* shear yield mechanism shape is completely different according to the continuity plate arrangement and connection type. For the case of test specimens *U*1-*FUW*1 and *U*1-*FW*1 with lower inclined continuity plate, the *PZ* yield mechanism involves the straight continuity plate and inclined continuity plate at the top and bottom of *PZ* boundaries, respectively. For the case of test specimens with straight continuity plates, i.e. *U*1-*FW*2 and *U*1-*FUW*2, the *PZ* yielding mechanism involves just the panel zone upper segment while for the case of specimen *U*1-*FUW*3, the *PZ* yielding mechanism extended into both the *PZ* upper and lower segments entirely. The *PZ* yield mechanism develops at the whole of the *PZ* area for the case of test specimen *U*1-*FUW*3.

For the case of test specimen *U*1-*FUW*3, the story drift angle reaches a value of 0.06 radians and shows the best performance, but specimen *U*1-*FW*3 has the worst performance of this ensemble and reaches a story drift angle of 0.04 radians prior to the undesirable fracture mode, i.e. the deep beam bottom flange fracture. The reasons for a better performance of test specimen *U*1-*FUW*3 are (1) straighter and clearer load path for the beams' bottom flanges, (2) better performance of flange plate connections compared to the cover plate connections (3) absence of middle continuity plate at this specimen (omission of extra fixity). These factors may be effective on more *PZ* contributions to the total *SMRF* deformations for this test specimen.

The asymmetric response shape (hysteresis loop) of the *PZ*, around the centre, could originate from the specimens' asymmetric geometry, so that the asymmetric hysteresis behaviour of the beams could, together with the shear strain values of the *PZ* (i.e. the *PZ* hysteresis behaviour), be an indicator of the non-uniform distribution of plastic strain in the lateral load transferring elements for the case of unequal beam depth. This means that, for such cases, there is an accumulation of plastic strain at the deep beam bottom flange. Based on the above-mentioned description, in the case of test specimen *U*1-*FUW*3, the hysteresis loops corresponding to the beams and the *PZ* had an approximately symmetric shape, see Figure (8) and Table (3). Regarding the largest *PZ* shear strain value (maximum *PZ* shear strain is 0.035), which provided a potential for more contribution to the total deformation, a more uniform plastic strain distribution, see strain gauges No. 1 and 6 in Figure (12), was expected, and there was a more balanced plastic strain distribution between the

Table 3. Experimental results.

Specimen Name	Drift Angle (Radians)	Shallow Beam Side		Deep Beam Side		Panel Zone							Test Observation
		Plastic Rotation		Plastic Rotation		Shear Strain		Minimum PZ Shear Strain at Story Drift Angle 0.04 Radians	Plastic Shear Strain		Maximum PZ Shear Strain at Story Drift Angle 0.04 Radians	*	
		Max	Min	Maxi	Min	Maxi	Min		Max	Min			
U1-FW1	0.05	0.038	-0.036	0.039	-0.036	0.026	-0.022	0.0181	0.019	-0.023	0.0216	.019	Deep Beam Bottom Flange Fracture
U1-FW2	0.05	0.041	-0.038	0.045	-0.043	0.014	-0.019	0.0112	0.011	-0.016	0.0162	.014	Deep Beam Bottom Flange Fracture
U1-FW3	0.04	0.024	-0.028	0.027	-0.037	0.021	-0.029	0.021	0.0175	-0.026	0.029	.021	Deep Beam Bottom Flange Fracture
U1-FUW1	0.06	0.043	-0.044	0.044	-0.046	0.034	-0.035	0.031	0.031	-0.031	0.0315	.026	Without any Failure Up to .06 Radians
U1-FUW2	0.05	0.034	-0.035	0.040	-0.038	0.033	-0.024	0.0208	0.023	-0.031	0.026	.024	Deep Beam Bottom Flange Fracture
U1-FUW3	0.06	0.042	-0.042	0.046	-0.046	0.035	-0.035	0.0317	0.033	-0.033	0.0317	.026	Without any Failure Up to .06 Radians

*(Asterisk) is Referred to Maximum Value of Gamma $\gamma;\gamma = \theta_{pz}(1 - d_c / L - d_b / h)$: L, H, D_b, D_c are Beam's Lengths, Column's Height, Beam's Section Depth, Column's Section Depth Respectively.

shallow beam, the deep beam and the *PZ*, so that the rupture was not expected. In the case of test specimen *U*1-*FW*2, which showed an asymmetric arrangement of hysteresis loops of the *PZ* response, and the smallest *PZ* shear strain value of this ensemble (0.014 radians), a deep beam fracture was expected, see Figure (8) and Table (3).

6. Conclusion

In this study, experiments of six full scale subassemblages with unequal beam depth were carried out in order to investigate the effect of connection detailing arrangements in the cyclic behavior and performance of welded connection moment resisting frames subjected to cyclic loading. The experiment revealed that a deep beam bottom flange fracture could be a premature failure mode before experiencing the story drift angle of 0.06 radians for *SMRF* with unequal beam depth. The reasons may be due to asymmetric geometry of the beams, *PZ* boundaries and connections arrangements around main column axis resulting in plastic strain accumulation at the intersection of the deep beam bottom flange and plate-reinforced connection ends, i.e. coverplate and flange plate and less contribution of *PZ* shear deformation originating from connection type and continuity plate arrangement. Flange plates with a haunch connection system, i.e. connection detailing arrangement of test specimen *U*1-*FUW*3, are the first alternative to eliminate the mentioned undesirable rupture mode. The connection detailing arrangement of test specimen *U*1-*FUW*1 could also be the second choice to exclude the mentioned rupture mode. The following conclusions can be drawn from the experiments:

- A combination of coverplate with straight continuity plate arrangement (i.e. test specimen *U*1-*FW*2) and flange plate with straight continuity plate arrangement (i.e. test specimen *U*1-*FUW*2) could not prevent an undesirable rupture mode and both test specimens fractured at a story drift angle of 0.05 radians. In other words, straight continuity plate arrangement is not a proper configuration to prevent the undesirable deep beam bottom flange fracture mode.
- None of the coverplate connections experienced a story drift angle of 0.06 radians, but some of the test specimens with flange plate connection, including *U*1-*FUW*3 and *U*1-*FUW*1, experienced a story drift angle of 0.06 radians without any rupture at the deep beam bottom flange. Therefore, there is a superiority of flange plate connection over coverplate connection regarding the seismic *SMRF* performance for unequal beam depth. The recommendations given in *FEMA*-350 [1] stipulate that the flange plate connection is superior to the coverplate connection with regard to the seismic performance of *SMRF* and confirm the findings of this study.
- Considering the *PZ* shear strain values for different connection detailing arrangements, different test specimens show that plate-reinforced connection types, i.e. coverplate and flange plate, have an important role in the control of *PZ* shear strain values. In other words, the specimens with flange plate have larger *PZ* shear strain values than the *PZ* shear strain values of the specimen with coverplate. None of the *PZ* shear strain values of test specimens with coverplate in this study, i.e. *U*1-*FW*1, *U*1-*FW*2 and *U*1-*FW*3, reached a value of 0.03 radians, while the *PZ* shear strain values of all specimens with flange plate, i.e. *U*1-*FUW*1, *U*1-*FUW*2 and *U*1-*FUW*3 had shear strain values larger than a value of 0.03 radians. Furthermore, the continuity plate arrangement has an important role in the control of the *PZ* shear strain value for unequal beam depths. In other words, the *PZ* shear strain value of the specimen with inclined continuity plate for the same type of plate-reinforced connection, i.e. coverplate or flange plate is larger than the case of test specimens with a straight continuity plate arrangement.
- The shallow beam of specimens with inclined continuity plate arrangement, i.e. test specimens *U*1-*FUW*1 and *U*1-*FW*1 hardly entered a nonlinear range based on the measured strain gauges on the shallow beam and cyclic response while the shallow beams for the rest of the test specimens especially in the case of test specimens with the haunch connection system exhibited severe nonlinearity. This showed that the inclined continuity plate does not provide enough stiffened support for the shallow beam.

7. Acknowledgments

This study was supported by the Structural Engineering Research Centre at *IIEES*, the International Institute of Earthquake Engineering and

Seismology (Grant No. 7360). The described tests were performed in the latter's Structural Laboratory. Much appreciation should be expressed to all the technicians and staff of the laboratory, especially H. Mortezaee, M. Javali, M. Jabbarzadeh, K. Gorji, and H. Farshchi without whose valuable help, this study could not have been performed.

References

1. FEMA (2000). "Recommended Seismic Design Criteria for New Steel Moment Frame Building", Report No. FEMA 350, Federal Emergency Management Agency.
2. FEMA (2000). "State of the Art Report on Welding and Inspection", Report No. FEMA-355B, Federal Emergency Management Agency.
3. FEMA (2000). "State of the Art Report on Connection Performance", Report No. FEMA-355D, Federal Emergency Management Agency.
4. AISC (2005). "Prequalified Connections for Special and Intermediate Steel Moment Frames for Seismic Applications", Chicago (IL), American Institute of Steel Construction.
5. Krawinkler, H., Bereto, V.V., and Popov, E.P. (1971). "Inelastic Behaviour of Steel Beam to Columns Subassemblagement", EERC Report No. 71-7, University of California, Berkeley.
6. Bertero, V.V., Krawinkler, H., and Popov, E.P. (1973). "Further Studies on Seismic Behaviour of Steel Beam-to-Column Subassemblages", EERC Report No. 73-27, Univ. of California, Berkeley.
7. Popov, E.P. (1987). "Panel Zone Flexibility in Seismic Moment Joints", *J. Constr. St. Res.*, **8**, 91-118.
8. Tsai, K.C. and Popov, E.P. (1988). "Steel Beam-Column Joints in Seismic Moment Resisting Frames", UCB/EERC Report No. 89/19, University of California, Berkeley.
9. International Conference of Building Officials (ICBO) (1988). "Uniform Building Code", ICBO, Whittier (CA).
10. El-Tawil, S. (1999). "Inelastic Behavior and Design of Steel Panel Zones", *J. Struct. Eng.*, **125**(2), 183-193.
11. El-Tawil, S. (2000). "Panel Zone Yielding in Steel Moment Connections", *Engineering Journal,* Third Quarter.
12. Federal Emergency Management Agency (FEMA) (1995). "Internal guidelines: Evaluation, Repair, Modification, and Design of Welded Steel Moment-Frame Structures", Report FEMA-267, Prepared by the SAC Joint Venture for FEMA, Washington, D.C.
13. Lee, C.-H. and Uang, C.-M. (1997). "Analytical Modeling of Dual Panel Zone in Haunch Repaired Steel Moment-Resisting Frames", *Journal Struct. Eng., ASCE,* **123**(1), 20-29.
14. AISC (1997). "Seismic Provisions for Structural Steel Buildings", American Institute of Steel Construction, Chicago (IL).
15. Jin, J. and El-Tawil, S. (2005). "Evaluation of FEMA 350 Seismic Provisions for Steel Panel Zones", *J. Strut. Eng., ASCE*, **131**(2), 250-258.
16. Civjan, S.A., Engelhardt, M.D., and Gross, J.A., (2000). "Retrofit of Pre-Northridge Moment-Resisting Connections", *J. Struct. Eng.*, **126**, 445-452.
17. Qi-Song, Uang, Chia-Ming,and Gross, J. (2000). "Seismic Rehabilitation Design of Steel Moment Connection with Welded Haunch", *J. Struct. Eng.*, **126**, 69-78.
18. Chi, B., Uang, Ch.-M., and Chen, A. (2006). "Seismic Rehabilitation of Pre-Northridge Steel Moment Connections: A Case Study", *J. Constr. St. Res.*, **62**, 783-792.
19. Uang, Ch.-M., Bondad, D., and Lee, Ch.-H. (1998). "Cyclic Performance of Haunch Repaired Steel Moment Connections: Experimental Testing and Analytical Modeling", *Eng. Struct.*, **20**, 552-61.
20. Kim, T., Whittakar, A.S., Gilani, A.S.J., Bertero, V.V., and Takhirov, S.M. (2002). "Experimental Evaluation of Plate-Reinforced Steel Moment Resisting Connections", *J. Struct. Eng., ASCE*, **128**(4), 483-91.
21. Kim, T., Whittakar, A.S., Gilani, A.S.J., Bertero V.V., and Takhirov, S.M. (2002). "Cover-Plate and Flange-Plate Steel Moment-Resisting Connections", *J. Struct. Eng., ASCE*, **128**(4), 474-82.

22. Chou, C.-C. and Wu, Ch.-Ch. (2007). Performance Evaluation of Steel Reduced Flange Plate Moment Connections", *J. Eq. Eng. Struct. Dyna*., **36**, 2083-2097.

23. Engelhardt., M.D. and Sabol., T.A. (1998). "Reinforcing of Steel Moment Connections with Coverplates: Benefits and Limitations, Engineering Structures", *J. Struct. Eng., ASCE*, **20**(4-6), 510-20.

24. Nakishima, M., Tayetema, E., Morisako, K., and Suita, K. (1998). "Full-Scale Test of Beam-Column Subassemblages Having Connection Details of Shop-Welding Type", *Structural Engineering Worldwide*, Elsevier Science (CD-ROM), Paper Ref. T158-7.

25. El-Tawil., S., Mikesell., T., and Kunnath., S.K. (2000). "Effect of Local Details and Yield Ratio on Behavior of FR Steel Connections", *J. Struct. Eng., ASCE*, **126**(1), 79-87.

26. Dubina, D. and Stratan, A. (2002). "Behavior of Welded Connections of Moment Resisting Frames Beam to Column Joints", *Eng. Structs.*, **24**, 1431-40.

27. Hopperstad, O.S., Borvik, T., Langseth., M., Labibies., K., and Albertini, C. (2003). "On the Influence of Stress Triaxiality and Strain Rate on the Behavior of a Structural Steel, Part I. Experiments", *Europe. J. Mech. A/Solids*; **22**, 1-13.

28. Morquio, A. and Reira, J.D. (2004). "Size and Strain Rate Effects in Steel Structures", *Eng. Struct.*, **26**, 669-79.

29. Dexter R.J. and Melenderz, M.I. (2000). "Through-Thickness Properties of Column Flanges in Welded Moment Connections", *J. Struct. Eng., ASCE*, **126**(1), 24-31.

30. Ricles, J.M., Fisher, J.W., and Kaufmann, E.J. (2002). "Development of Improved Welded Moment Connections for Earthquake-Resistant Design", *J. Const. St. Res.*, **58**, 565-604.

31. Anderson, J.C., Duan, J., Xiao, Y., and Maranian, P. (2002). "Cyclic Testing of Moment Connections Upgraded with Weld Overlays", *J. Struct. Eng.*, **128**(4), 509-516.

32. Bonowitz, D. (1995). "Surveys and Assessment of Damage to Buildings Affected by the Northridge Earthquake of January 17, 1994", Report SAC 95-06, SAC Joint Venture, Richmond, California.

33. Kaufmann, E.J. and Fisher, J.W. (1996), "Fracture Analysis of Failed Moment Frame Welded Joints Produced in Full-Scale Laboratory Tests and Buildings Damaged in the Northridge Earthquake", Technical Report Number SAC 95-08, SAC Joint Venture, Richmond California.

34. Fisher, J.W. and Dexter, R.J. (1996). "Fatigue and Fracture", New York, McGraw-Hill, Chapter 8, LRFD Method.

35. Fisher, J.W., Dexter, R.J., and Kaufmann, E.J. (1997). "Fracture Mechanics of Welded Structural Steel Connections", Report Number SAC 95-09, FEMA-288.

36. Kaufmann, E.J. and Fisher, J.W. (1996). "Fracture Analysis of Failed Moment Frame Welded Joints Produced in Full-Scale Laboratory Tests and Buildings Damaged in the Northridge Earthquake", Technical Report Number SAC 95-08, SAC Joint Venture, Richmond California.

37. Kaufmann, E.J., Fisher, J.W., Di Julio, R.M., and Gross, J.L. (1997). "Failure Analysis of Welded Steel Moment Frames Damaged in the Northridge Earthquake", NISTIR 5944, National Institute of Standards and Technology, Gaithersburg, Md.

38. Ojdrovic, R.P. and Zarghamee, M.S. (1997). "A Repair Approach for Fractured Steel Moment Connections, Building to Last", *Proceeding, Structural Congress*, **XV**, Reston, VA, Structural Engineering Institute, 596-601.

39. AISC (2005). "Seismic Provisions for Structural Steel Buildings", Chicago (IL), American Institute of Steel Construction.

40. AWS (2002). "Structural Welding Code-Steel", Miami (FL), American Welding Society.

41. AISC (2005). "Specification for Structural Steel Buildings", Chicago (IL), American Institute of Steel Construction.

42. FEMA (1996). "Experimental Investigations of Beam-Column Sub Assemblages", Federal Emergency Management Agency Report SAC-96-01, Part 1, SAC Joint Venture, Sacramento (CA).